






RESEARCH ARTICLE | NOVEMBER 01 2022

Order of magnitude reduction in Joule heating of single molecular junctions between graphene electrodes

Gen Li ; Bing-Zhong Hu ; Wen-Hao Mao; Nuo Yang ; Jing-Tao Lü  



J. Chem. Phys. 157, 174303 (2022)

<https://doi.org/10.1063/5.0118952>



Nanotechnology & Materials Science



Optics & Photonics



Impedance Analysis



Scanning Probe Microscopy



Sensors



Failure Analysis & Semiconductors



Unlock the Full Spectrum.
From DC to 8.5 GHz.

Your Application. Measured.

[Find out more](#)

 Zurich Instruments

Order of magnitude reduction in Joule heating of single molecular junctions between graphene electrodes

Cite as: *J. Chem. Phys.* **157**, 174303 (2022); doi: [10.1063/5.0118952](https://doi.org/10.1063/5.0118952)

Submitted: 7 August 2022 • Accepted: 10 October 2022 •

Published Online: 1 November 2022



View Online



Export Citation



CrossMark

Gen Li,¹  Bing-Zhong Hu,¹ Wen-Hao Mao,¹ Nuo Yang,²  and Jing-Tao Lü^{1,a)} 

AFFILIATIONS

¹School of Physics, Institute for Quantum Science and Engineering, and Wuhan National High Magnetic Field Center, Huazhong University of Science and Technology, Wuhan 430074, China

²State Key Laboratory of Cool Combustion, and School of Energy and Power Engineering, Huazhong University of Science and Technology, Wuhan 430074, China

^{a)} Author to whom correspondence should be addressed: jtlu@hust.edu.cn

ABSTRACT

Maintaining stability of single-molecular junctions (SMJs) in the presence of current flow is a prerequisite for their potential device applications. However, theoretical understanding of nonequilibrium heat transport in current-carrying SMJs is a challenging problem due to the different kinds of nonlinear interactions involved, including electron–vibration and anharmonic vibrational coupling. Here, we overcome this challenge by accelerating Langevin-type current-induced molecular dynamics using machine-learning potential derived from density functional theory. We show that SMJs with graphene electrodes generate an order of magnitude less heating than those with gold electrodes. This is rooted in the better phonon spectral overlap of graphene with molecular vibrations, rendering harmonic phonon heat transport being dominant. In contrast, in a spectrally mismatched junction with gold electrodes, anharmonic coupling becomes important to transport heat away from the molecule to surrounding electrodes. Our work paves the way for studying current-induced heat transport and energy redistribution in realistic SMJs.

Published under an exclusive license by AIP Publishing. <https://doi.org/10.1063/5.0118952>

I. INTRODUCTION

Recent development of the scanning thermal probe technique has enabled experimental measurement of thermal conductance across single-molecular junctions (SMJs) and metallic atomic chain junctions,^{1–5} one and two decades later than the first thermoelectric⁶ and electrical⁷ measurements, respectively. This opens exciting opportunities for systematic investigation of thermal transport in atomic-scale junctions, i.e., through chemical engineering.^{8–19}

A more challenging problem is nonequilibrium thermal transport between electronic and vibrational/phononic degrees of freedom in the presence of electrical current.²⁰ Wherein, two important bottleneck processes controlled by electron–vibration/phonon and anharmonic phonon interaction are simultaneously at play. First, electrons transfer energy to the molecular vibrations via electron–vibration interaction. Second, the excess energy is redistributed within molecular vibrational modes and further transported

to the surrounding electrodes, in which anharmonic vibrational coupling may play a key role. This hybrid heat transport problem is quite different from the normal phonon heat transport study where heat current is driven by the temperature difference between two baths.

For a comprehensive understanding of this problem, both of the above-mentioned processes need to be addressed on an equal footing. Theoretical studies of the former have revealed at least two energy transfer mechanisms:^{21,22} stochastic Joule heating and work performed by a deterministic non-conservative current-induced force. While Joule heating is always present, the non-conservative current-induced force becomes important in high conductance SMJs. Experimentally, the signature of Joule heating has been probed by electrical and optical methods,^{23–26} while only preliminary evidence of current-induced non-conservative force has been reported.²⁷ On the other hand, studies on vibrational energy redistribution within the molecule and subsequent energy transport

to the electrodes are scarce due to the expensive computational cost required to study realistic SMJs.²⁸

In this work, we overcome this difficulty by employing machine-learning potential derived from *ab initio* molecular dynamics (MD) data. We perform a comparative study on the heat transport properties of alkane and carbon chain junctions with gold and graphene electrodes. Our results show that good spectral overlap between molecular vibrations and graphene phonons ensures effective harmonic energy transport between them and results in much less heating of the molecule as compared to gold electrodes. However, in junctions with gold electrodes, anharmonic vibrational coupling is essential to enhance the efficiency of heat transport to the electrodes. Our work highlights the importance of vibrational spectral overlap in enhancing heat transport at the single molecule level and demonstrates the superior advantage of graphene as electrodes for constructing stable SMJs.^{29–31}

II. THEORY

A. System setup

A schematic diagram of the setup is shown in Fig. 1(a). In our theoretical framework, we divide the whole junction into electron and phonon subsystems. Each subsystem is further divided into the left and right baths and the central molecule. In the electron subsystem, the voltage bias is applied between the two electrodes by shifting their chemical potentials. Driven by the voltage bias, electrons transport across the molecule between the two electrodes, during which they may interact with molecular vibrations in the phonon subsystem and result in energy transfer between them. Since the molecule is the bottleneck part of electron and heat transport, we only consider coupling of the two subsystems within the molecule [within the dashed boxes in Fig. 1(b)]. This setup has been widely used in the study of Joule heating in single molecular junctions.

In our theory based on a semiclassical Langevin equation, following the standard open system approach, we choose the system

as atomic degrees of freedom (DoF) within an extended molecule, which can include some of the electrode atoms [solid boxes in Fig. 1(b)]. The whole electron subsystem is treated as a nonequilibrium bath carrying electrical current. It couples to the system through electron–vibrational interaction within the dashed boxes. The boundary atoms of the system under the blue lines couple to the left and right phonon baths. The baths DoF are auxiliary and characterized by the coupling matrix defined in Sec. II B. The phonon baths stay in thermal equilibrium throughout the whole process. Energy transport from the electron bath to the system takes place once the electron bath is driven out of equilibrium by applied voltage. The excess energy is further transported to the two phonon baths. The main focus of this work is to perform comparative study on this energy transport process in two types of single molecular junctions with gold and graphene electrodes.

B. The semiclassical Langevin equation

Our theory is based on a semiclassical Langevin equation^{32–36}

$$\ddot{\mathbf{Q}} = -\nabla_{\mathbf{Q}}V - \Gamma \cdot \dot{\mathbf{Q}} - \mathbf{A} \cdot \mathbf{Q} + \mathbf{f}, \quad (1)$$

which takes a similar form as the classical Langevin equation. The details of its derivation can be found in Ref. 32. To arrive at Eq. (1), we have made the following two important approximations: (1) We ignore the energy dependence of the electronic density of states, such that the Markovian approximation holds (see discussions in Sec. II C). (2) The displacement of atoms away from their equilibrium positions is small enough such that the average molecule structure does not deviate much from the equilibrium one. In this way, we do not need to update the electron–vibration coupling or the electronic structure during MD on the fly, thus ignoring their \mathbf{Q} dependence. Despite these approximations, as we explain in the following, it extends the classical version in two aspects: (1) We treat the electron and phonon baths quantum-mechanically, which follow

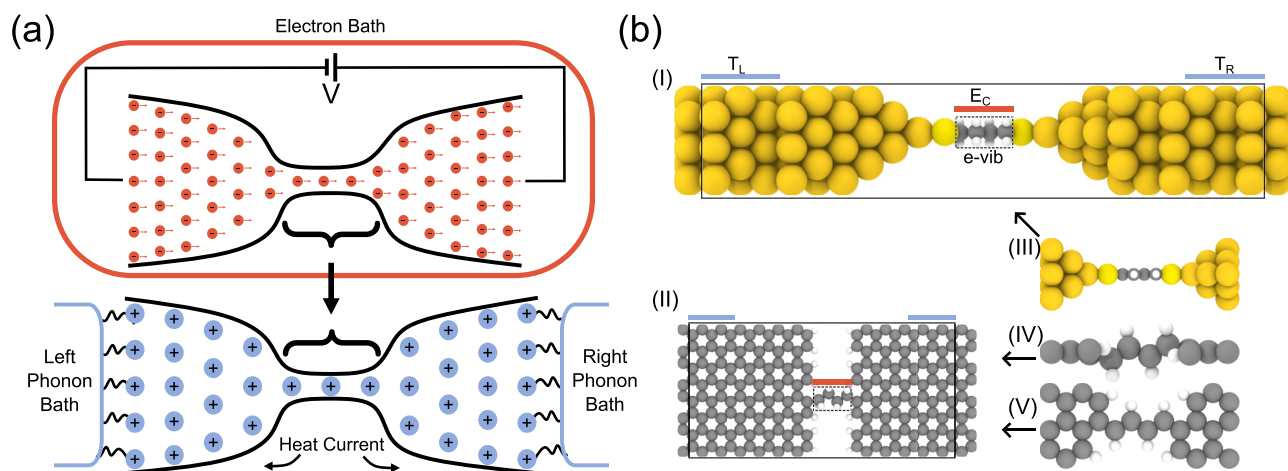


FIG. 1. (a) Schematic of the theoretical model. (b) Structures of molecular junctions considered in this work. We consider two types of molecular structures with CH_2 (I, II) and CH (III, IV, V) units, respectively. The electrodes are either gold (I, III) or graphene (II, IV, V). For gold junction, the molecule bonds to gold through sulfur atoms. For graphene junction, the molecule bonds directly through C–C bonds. OVITO³⁸ is used for visualization.

Fermi–Dirac and Bose–Einstein statistics, respectively. (2) We allow the electron bath to be out of thermal equilibrium.

The vector \mathbf{Q} is a mass-normalized displacement vector containing all the atomic DoF of the system, corresponding to atoms within the solid boxes in Fig. 1(b). The first term on the right-hand side (r.h.s.) accounts for the force exerted on the system atoms due to the atomic potential. Each of the rest terms at r.h.s. includes contributions from the electronic and phononic baths, i.e., $\mathbf{\Gamma} = \mathbf{\Gamma}_L + \mathbf{\Gamma}_R + \mathbf{\Gamma}_e$. According to previous results on current-induced forces in molecular junctions,³² we can divide $\mathbf{\Gamma}$ and \mathbf{A} into symmetric and anti-symmetric parts, respectively. The symmetric part of $\mathbf{\Gamma}$ represents the friction contributed by all baths. The anti-symmetric part comes from the electronic bath and is non-zero only when there is a non-zero electrical current. It represents the Lorentz-like force from an effective magnetic field due to the Berry phase of nonequilibrium electrons.^{22,37} The symmetric part of \mathbf{A} represents renormalization of the potential due to coupling to the baths, including contributions from all the baths. However, the anti-symmetric part of \mathbf{A} comes solely from the current-carrying electronic bath and becomes zero in thermal equilibrium at zero voltage bias. It represents the non-conservative current-induced forces.^{21,22,37} We have checked that for the molecular junctions considered in this work, the anti-symmetric parts of $\mathbf{\Gamma}$ and \mathbf{A} are negligible due to the small electrical conductance of the junctions. The final term \mathbf{f} represents fluctuating forces with contributions from all baths. Different from the classical Langevin equation, here \mathbf{f} includes quantum zero-point fluctuations. The phonon and electron DoF follow quantum Bose–Einstein and Fermi–Dirac statistics, respectively. When the electron bath is driven to nonequilibrium, \mathbf{f}_e also has corresponding nonequilibrium fluctuations that are responsible for Joule heating.^{22,37} Since the two phonon baths are in thermal equilibrium, any fluctuating force contributed by them is connected to the corresponding friction force through the fluctuation–dissipation relation. However, when there is an electrical current, the fluctuation–dissipation relation does not hold anymore for the electron bath.

C. Numerical calculation

To perform MD simulation using Eq. (1), we need to calculate the potential and the coupling parameters for all the baths. We can express all the needed coupling parameters using self-energies in the nonequilibrium Green’s function (NEGF) theory,³⁷ i.e., in the frequency domain,

$$\mathbf{\Gamma}(\omega) = -\text{Im}\mathbf{\Pi}^r(\omega)/\omega, \quad \mathbf{A}(\omega) = \text{Re}\mathbf{\Pi}^r(\omega). \quad (2)$$

The fluctuating force \mathbf{f} is characterized by the time correlation function^{32,37}

$$\langle \mathbf{f}_\mu(t) \mathbf{f}_\nu^T(t') \rangle = \frac{i}{2} \hbar \delta_{\mu,\nu} [\mathbf{\Pi}_\mu^>(t-t') + \mathbf{\Pi}_\mu^<(t-t')], \quad \mu, \nu = L, R, e. \quad (3)$$

Here, $\mathbf{\Pi}^r$, $\mathbf{\Pi}^>$, and $\mathbf{\Pi}^<$ are the retarded, greater, and less self-energies in the NEGF theory,^{32,37} with $\mathbf{\Pi}^r = \mathbf{\Pi}_e^r + \mathbf{\Pi}_R^r + \mathbf{\Pi}_L^r$.

In general, the frequency dependence of $\mathbf{\Gamma}(\omega)$ and $\mathbf{A}(\omega)$ translates into a convolution in time between $\mathbf{\Gamma}\text{-}\mathbf{Q}$ and $\mathbf{A}\text{-}\mathbf{Q}$, resulting in a generalized Langevin equation with a memory effect. Here, the Markovian approximation made in Eq. (1) corresponds to ignoring the frequency dependence of $\mathbf{\Gamma}$ and \mathbf{A} . For the phonon baths, this approximation can be improved by including more electrode

atoms in the extended molecule.^{39,40} For the electronic bath, it is a good approximation for molecular junction with gold electrodes. For graphene electrodes, due to the linear energy dependence of the electronic density of states, we should, in principle, keep the frequency dependence. Here, we focus on the ability of the molecule to transfer excess energy injected from the electron bath to the surrounding phonon baths. For the ease of comparison between the two types of junctions, we chose to use the same approximation for them. Our main conclusion is not sensitive to this approximation.

In the numerical calculation, we use a phenomenological model to treat the coupling of the system [via atoms under blue lines in Fig. 1(b)] to the two phonon baths. The coupling of the system to each phonon bath is approximated by one diagonal friction matrix with the same diagonal element $\gamma_{L/R} = 10 \text{ ps}^{-1}$. As mentioned above, the accuracy of this approximation can be systematically improved by including more electrode atoms in the extended molecule to account for non-Markovian memory effects. For the electron bath, first-principles calculation at the density functional theory (DFT) level is used to calculate the electronic structure of the whole electron subsystem, molecular vibrational modes, and electron–vibration interaction within the molecule [dashed boxes in Fig. 1(b)], based on which the NEGF self-energies are evaluated. The SIESTA-TransSIESTA-Inelastica toolkit is used for this purpose.^{41–43} We have used quantities calculated at zero bias. The voltage bias is applied by simply shifting the left and right electrode chemical potential in the corresponding Fermi distribution. This can be improved in the future by calculating these parameters at a finite voltage. For the potential, we use the machine-learning potentials trained by *ab initio* MD data of the same structure with the help of the DeePMD-kit.⁴⁴ The obtained potential can accurately reproduce the vibrational modes of each structure from DFT (see Fig. 2). Without losing numerical accuracy, we can perform MD simulation at a speed of $\sim 1\text{--}2$ orders of magnitude faster than standard *ab initio* MD.²⁸ Results shown below are obtained by averaging three independent MD runs, where each run lasts for 4 ns, with a MD time step of $dt = 0.5 \text{ fs}$. Such calculations are not feasible for *ab initio* MD due to the expensive computational cost. We use fixed boundary conditions in the transport direction by fixing atoms in the outermost layers and periodic boundary conditions in the perpendicular direction. A schematic diagram of our numerical procedure is depicted in Fig. 3.

From the MD trajectory, we can calculate the kinetic energy power spectrum of the system, defined as

$$C_{vv}(\omega) = \sum_i C_{v_i v_i}(\omega) = \sum_i \int dt C_{v_i v_i}(t) e^{i\omega t}, \quad (4)$$

where

$$C_{v_i v_i}(t) = \langle v_i(t) v_i(0) \rangle = \frac{1}{T_0} \int dt' v_i(t'+t) v_i(t') \quad (5)$$

is the velocity correlation function at steady state. The integration is over a time range of length T_0 after the system reaches steady state. A cumulative integration of the power spectrum quantifies the contribution of each frequency range to the total kinetic energy,

$$E_K(\omega) = \int_0^\omega d\omega' C_{vv}(\omega'). \quad (6)$$

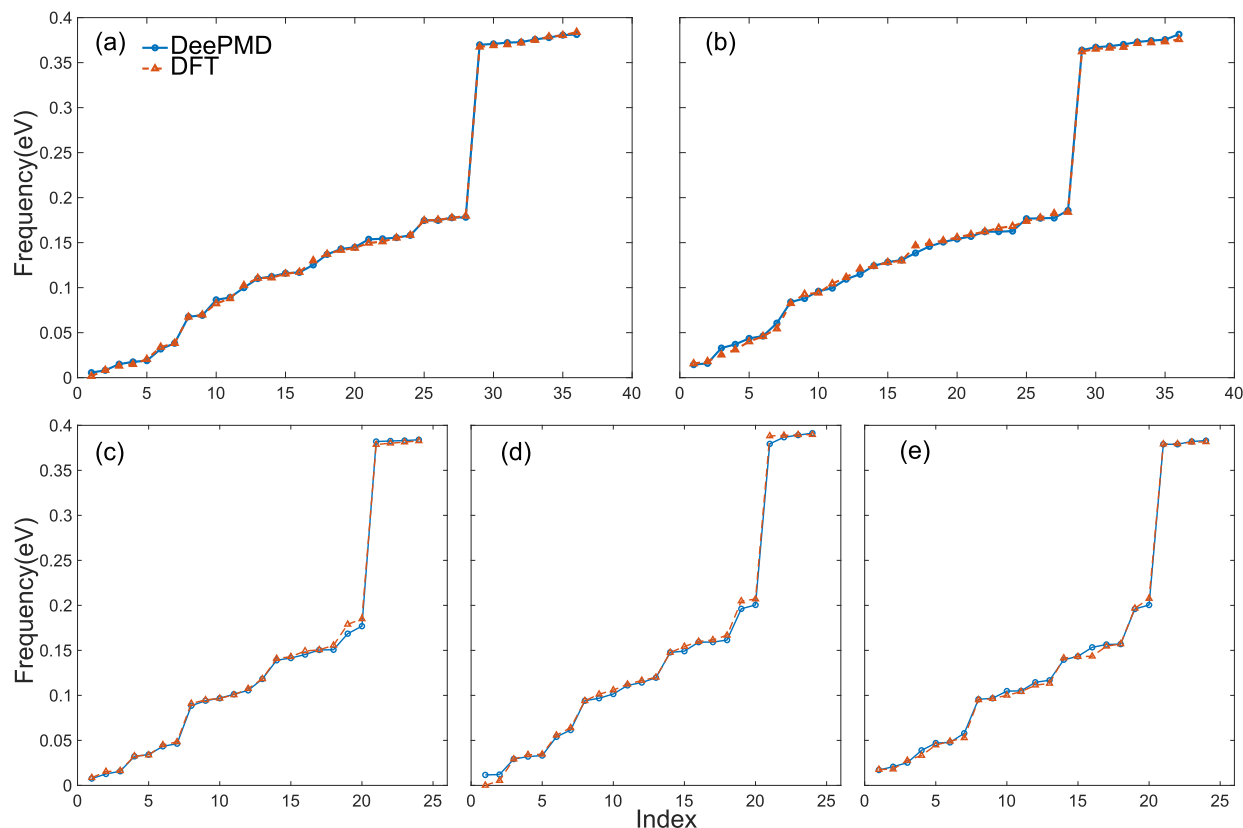


FIG. 2. Comparison of molecular vibrational frequencies from machine-learning potential and DFT. The vibrational modes of atomic DoF within the dashed boxes in Fig. 1(b) are calculated using the finite difference method. During the calculation, all atoms except those in the dashed boxes are fixed. [(a)–(e)] corresponds to structures shown in Fig. 1(b) (I–V). Blue circles are results from DeePMD, and red triangles are from DFT.

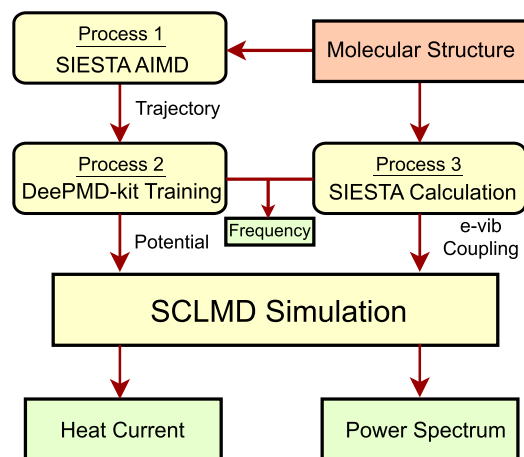


FIG. 3. Work flow diagram. The red arrows present the workflow. After DeePMD-kit training of SIESTA molecular dynamics (MD) data and DFT (SIESTA-TransSIESTA-Inelastica toolkit) calculation of the electronic structure, vibrational spectrum, and electron–vibration coupling, the parameters are passed to a homemade MD package based on the semi-classical Langevin equation to perform current-induced MD. The power spectrum and heat current are obtained from the resulting MD trajectories.

Since the definition of temperature in such atomic-scale systems in a nonequilibrium situation is not unambiguous,⁴⁵ we characterize heating of the molecule by the excess kinetic energy ΔE_K , which is the difference of molecular kinetic energy at 1 and 0 V. From the MD trajectories, we can also calculate the heat current injected from different baths,

$$I_\alpha = \frac{1}{T_0} \int_0^{T_0} dt \mathbf{F}_\alpha(t) \cdot \dot{\mathbf{Q}}(t), \quad (7)$$

where $\mathbf{F}_\alpha = -\Gamma_\alpha \dot{\mathbf{Q}} - \mathbf{A}_\alpha \mathbf{Q} + \mathbf{f}_\alpha$ is the total force acting on the system from bath α . The integral is over the time range of length T_0 when the system reaches a steady state.

III. RESULTS AND DISCUSSIONS

Our main results are summarized in Fig. 4. Two types of molecule junctions with sp^2 and sp^3 hybridization with gold and graphene electrodes are considered at a voltage bias of 1 V. The molecule structures are shown in Fig. 1(b). To show the robustness of our results, we consider a wide range of electrical conductance by manually shifting the average chemical potential. We observe an order of magnitude more heating in gold junction compared to graphene junction, independent of the type of molecule or

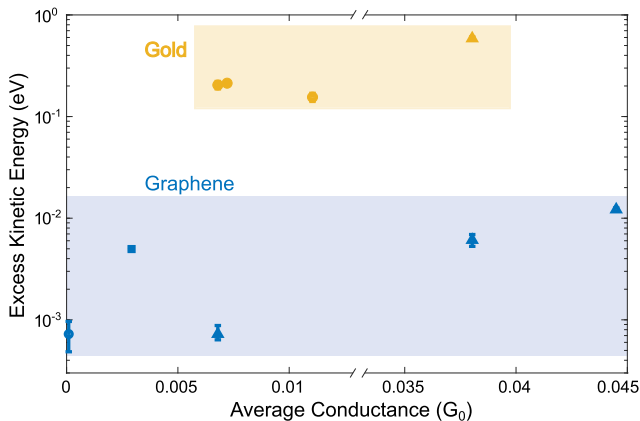


FIG. 4. Excess kinetic energy of the central molecule for junctions with different conductance between gold (yellow) and graphene (blue) electrodes at a voltage bias $V = 1$ V. The heating of gold junctions is ~ 1 – 2 orders of magnitude larger than that of graphene junctions. The circle points are results from alkane (CH_2) structures, and triangle and square points are from carbon chain (CH) structures shown in Fig. 1(b).

electrical conductance. In the following, we show that less heating of the graphene junction is rooted in better spectral overlap between molecular vibrations and graphene phonons. This results in efficient harmonic energy transport to surrounding electrodes and less heating of the molecule.

To further unravel these results, we analyze heating of the system in the vibrational mode space. Microscopic processes of energy transfer between the electron bath and the system are the emission and absorption of molecular vibrational quanta during inelastic electron tunneling. We define an excitation efficiency to quantify these processes for each vibrational mode n ,

$$\gamma_n = \hbar\omega_n \frac{\chi_{nm}^+}{\eta_{nm}}. \quad (8)$$

Here, $\hbar\omega_n$ is the energy of vibrational mode n , χ_{nm}^+ and η_{nm} characterize the nonequilibrium excitation and damping of the vibrational mode due to coupling to nonequilibrium electrons. In the Markovian approximation, they are written as³⁷

$$\chi_n^+ = \pi^{-1} \text{Re Tr}[M^n A_L(\mu_0) M^n A_R(\mu_0)], \quad (9)$$

$$\eta_n = (2\pi)^{-1} \text{Re Tr}[M^n A(\mu_0) M^n A(\mu_0)] = \Gamma_{e,nn}. \quad (10)$$

The excitation process only involves inelastic electronic transitions between left and right scattering states. Meanwhile, the damping process involves electronic transitions with initial and final states being from either the left or right. Here, $A = A_L + A_R$ is the total spectral function, with A_α spectral function due to scattering states from electrode α , and M^n is the electron–vibrational coupling matrix for vibrational mode n . We note that the vibrational modes and their coupling to electrons depend on the junction structures. Even the same molecule could have slight different vibrational modes and coupling matrix when it is put into different types of electrodes.

Figure 5 shows the excitation efficiency of alkane junctions with gold (a) and graphene (b) electrodes. Modes with blue color lie within the phonon band width of the electrodes, while those with red color are outside of the band width. Harmonic phonon energy transport from the blue modes to the two electrodes is the most effective channel to conduct excess energy out of the molecule (harmonic channel). Excess energy stored in red modes has to be down-converted into lower frequency modes via anharmonic interaction before being transferred to electrodes (anharmonic channel). For gold junction, the harmonic channel is much less efficient since the vibrational modes that interact strongly with electrons are all outside the energy range of the harmonic channel. Meanwhile, for

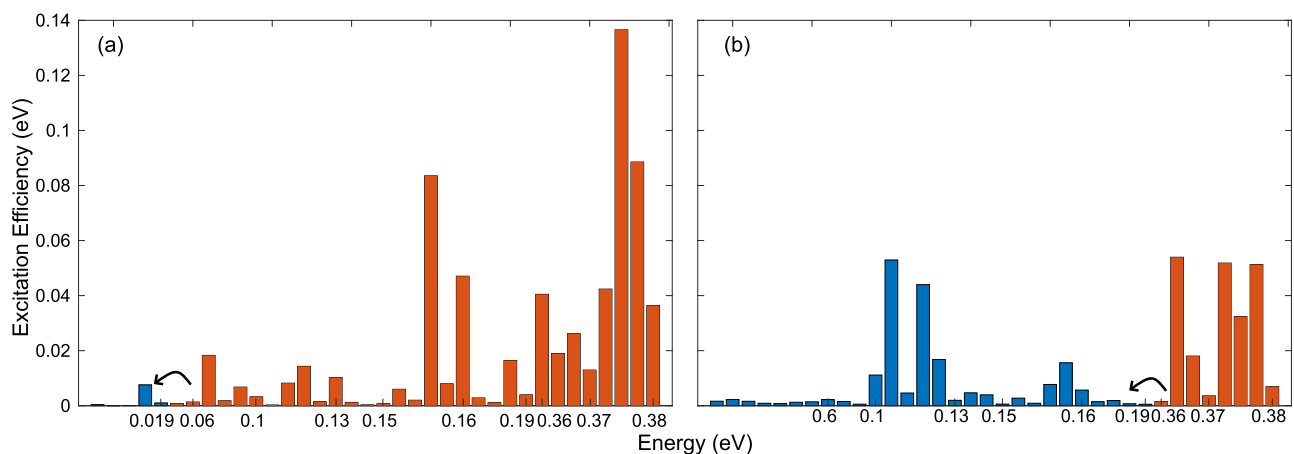


FIG. 5. Electronic excitation efficiency of molecular vibrational modes [Eq. (8)] for gold (a) and graphene (b) junctions. Blue modes have direct frequency overlap with electrode phonons. Energy transport through these modes to surrounding electrodes is mainly harmonic. Meanwhile, red modes have frequencies higher than the phonon band width. Thus, anharmonic frequency down-conversion is necessary before their excess energy is transported to surrounding electrodes (arrows).

graphene junction, only C–H stretching modes (>0.3 eV) are out of the graphene phonon band. Thus, effective harmonic energy transport is expected in the graphene junction.

The above analysis is confirmed by analyzing the kinetic energy power spectra of the molecule obtained from MD simulation in Fig. 6. The power spectra within the electrode phonon bandwidth show broadening due to coupling to electrode phonons, which is within $[0, 0.2]$ eV for graphene electrodes, but only within $[0, 0.02]$ eV for gold electrodes. Better spectral overlap between molecular vibrations and electrode phonons results in only observable heating of the C–H bond (>0.3 eV) for graphene junction. The situation is drastically different for gold junction, where heating in a much wider frequency range is observed. This is consistent with Fig. 5. The harmonic channel is much less effective in gold junction since the vibrational modes that overlap with the gold phonon band are much less excited than those outside the phonon band.

The steady state spectral distribution is a result of balance between energy input from the nonequilibrium electron bath and output to two surrounding phonon baths. To further disentangle these two effects, we have performed an extra simulation of the graphene junction using electron coupling parameters from the gold junction. The results are shown as red curves in Fig. 6 [see also Figs. 7(c)–Figs. 7(e) and 8]. More heating and a larger heat current (Fig. 8) can be observed in this case. But, the excess energy is still much smaller than the gold junction. Thus, we conclude that the smaller heating in graphene junction is mainly due to the

better frequency overlap of the molecular vibrations with two phonon baths. The effect of anharmonic channel can be deduced by comparing results using the anharmonic machine-learning potential [Figs. 6(a)–6(c)] and the harmonic approximation [Figs. 6(d)–6(f)]. The harmonic force is calculated from the dynamical matrix of the system obtained from the DFT calculation. The excess kinetic energy drops by more than 50% for both junctions when including anharmonic vibrational coupling.

Excessive heating of the molecule can also be studied within real space (Fig. 7). Previous studies have reported that asymmetric energy distribution in metal atomic chains (atomic hot-spot) originates from deterministic energy transfer of non-conservative current-induced force.⁴⁶ Normally, this requires that the junction have a high conductance ($\sim 1 G_0$). But the conductance of the molecular junctions we consider here is much lower. The effect of the non-conservative force is negligible, and we obtain a quite symmetric energy distribution. The asymmetry distribution of H atoms in Fig. 7(c) is possibly due to the structure asymmetry instead of the effect of current-induced forces.

We now turn to the heat current from the electron bath to the system (Fig. 8). In Fig. 8(a), the temperature of the electron bath increases from 300 K to 800 K at zero voltage bias while keeping the phonon bath temperature fixed at 300 K. In Fig. 8(b), voltage bias is applied to electrons between the left and right electrodes while keeping the temperature at 300 K. A temperature bias of ~ 400 K is needed to generate a similar heat current at $V = 1$ V. Comparing

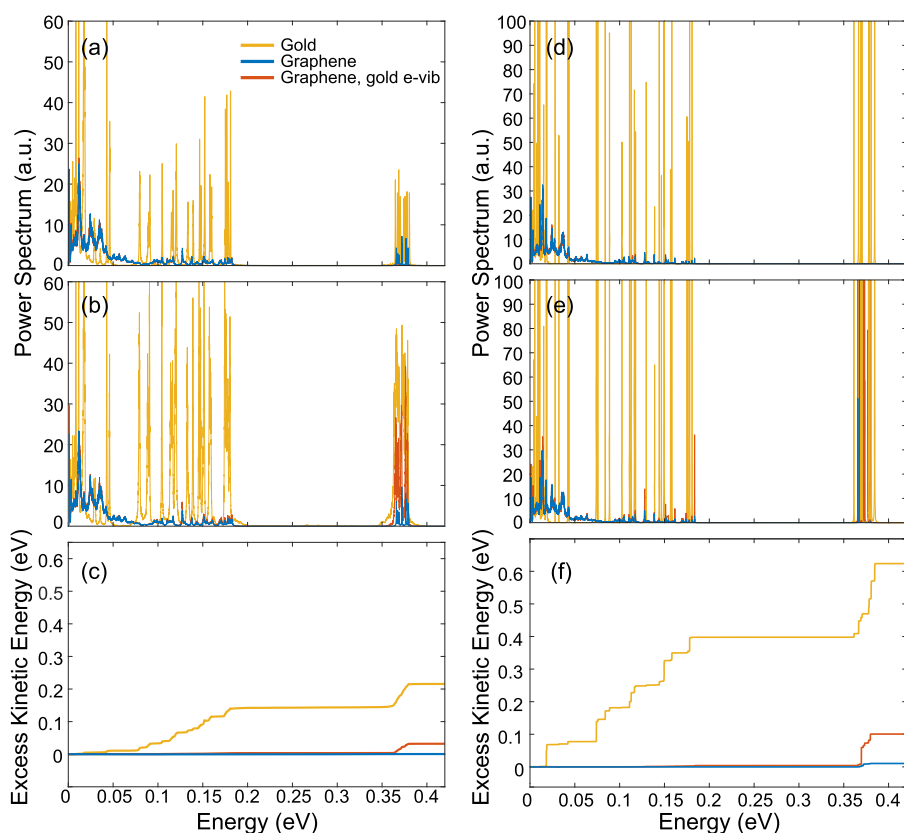


FIG. 6. Kinetic energy power spectra $C_{vv}(\omega)$ [Eqs. (4)–(6)] of the molecule at $V = 0$ V [(a) and (d)], $V = 1$ V [(b) and (e)], and the corresponding cumulative integration of the excess kinetic energy $\Delta E_K(\omega) = \int_0^\omega d\omega' [C_{vv}(\omega', 1 \text{ V}) - C_{vv}(\omega', 0 \text{ V})]$ [(c) and (f)] of the central molecule between gold and graphene electrodes. [(a)–(c)] and [(d)–(f)] are results obtained from the machine-learning potential and the harmonic potential, respectively. The yellow and blue lines are the results obtained from gold and graphene electrodes, respectively. The red lines are the results of graphene electrodes but with electron–vibration interaction from gold junctions. To get a larger current, we have shifted the Fermi level of graphene electrodes to 0.3 eV.

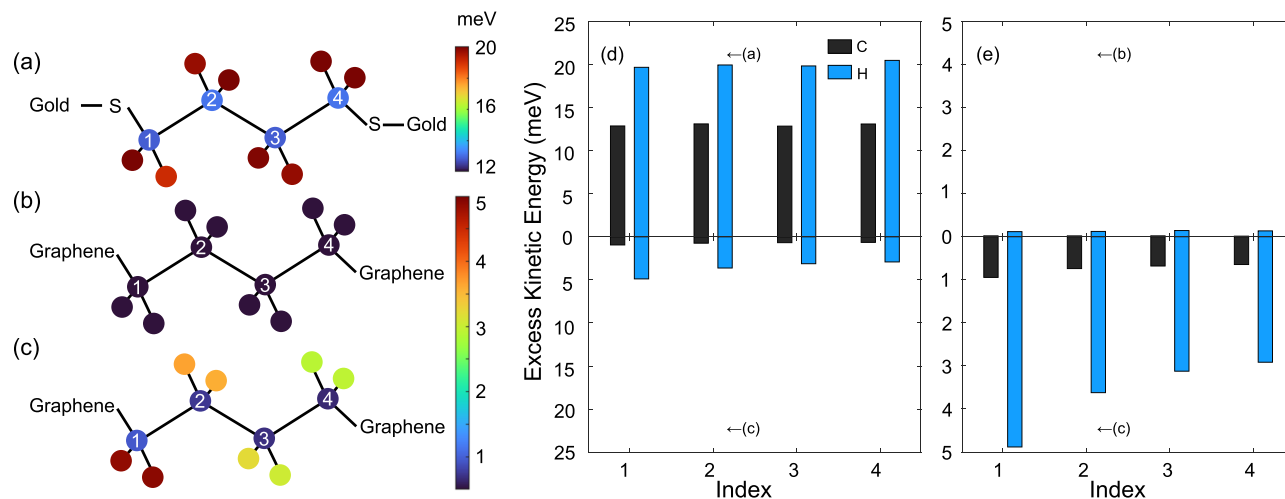


FIG. 7. Real-space excess kinetic energy distribution within the molecule for different electrodes and electron–vibration coupling. (a) and (b) Results for gold and graphene electrodes, respectively. (c) Results for an artificial graphene junction where the phonon subsystem is the same as (b), but the electron subsystem and its coupling phonons are taken from the gold junction (a). By comparing (c) with (b) and (a), we can disentangle two factors that determine the excess kinetic energy distribution: one is energy transfer from the electron bath to the system, and the other is energy transfer from the system to two phonon baths. (d) Comparison between (a) and (c). (e) Comparison between (b) and (c). Note the different scales of the y axis, and data below and above zero of y axis are both positive. They are plotted in opposite directions for ease of comparison.

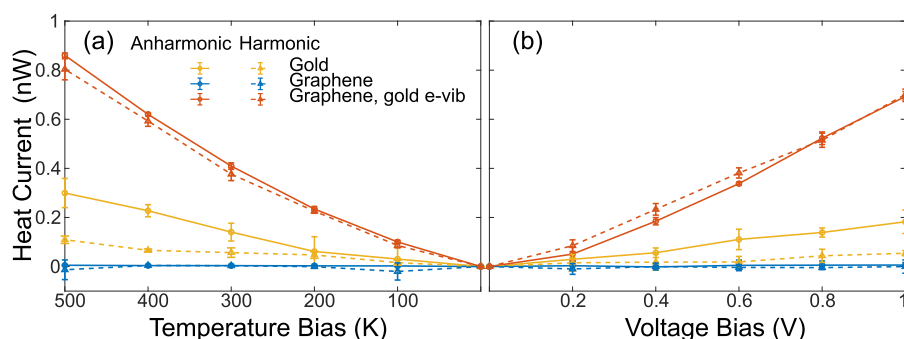


FIG. 8. Heat current as a function of temperature bias applied between electron and phonon systems (a) and voltage bias applied between two electrodes (b). Circles are obtained from anharmonic SCLMD using machine-learning potentials, while triangles are obtained from harmonic calculation, where the potential is calculated from the system dynamical matrix obtained from DFT. The color code is the same as in Fig. 6.

between the two types of junctions, anharmonic coupling is more important in gold junctions. Heat current increases by $>100\%$ when including the anharmonic coupling. While, for graphene electrodes, the harmonic and anharmonic results differ only slightly, indicating a negligible role of the anharmonic effect. The difference lies again in the spectral overlap between molecules and electrodes.

IV. CONCLUSION

In conclusion, with the help of machine learning potential with accuracy comparable to density functional theory, we have performed a systematic study on current-induced energy transport between electrons and phonons in SMJs. We show that better spectral overlap between electrode phonons and molecular vibrations makes graphene electrodes a promising candidate for developing stable single-molecular devices. Our work paves the way for studying current-induced molecular dynamics^{47,48} and nonequilibrium heat transport between electrons and phonons in realistic SMJs.

ACKNOWLEDGMENTS

This work was supported by the National Natural Science Foundation of China (Grant Nos. 22273029 and 21873033). We thank the National Supercomputing Center in Shanghai for providing computational resources.

AUTHOR DECLARATIONS

Conflict of Interest

The authors have no conflicts to disclose.

Author Contributions

Gen Li: Data curation (lead); Formal analysis (equal); Validation (equal); Visualization (lead). **Bing-Zhong Hu:** Data curation (supporting). **Wen-Hao Mao:** Data curation (supporting).

Nuo Yang: Supervision (supporting). **Jing-Tao Lü:** Conceptualization (lead); Formal analysis (equal); Funding acquisition (lead); Investigation (lead); Methodology (lead); Project administration (lead); Resources (lead); Software (lead); Supervision (lead); Validation (equal); Writing – original draft (lead); Writing – review & editing (lead).

DATA AVAILABILITY

The data that support the findings of this study are available from the corresponding author upon reasonable request.

REFERENCES

- L. Cui, W. Jeong, S. Hur, M. Matt, J. C. Klöckner, F. Pauly, P. Nielaba, J. C. Cuevas, E. Meyhofer, and P. Reddy, “Quantized thermal transport in single-atom junctions,” *Science* **355**, 1192 (2017).
- N. Mosso, U. Drechsler, F. Menges, P. Nirmalraj, S. Karg, H. Riel, and B. Gotsmann, “Heat transport through atomic contacts,” *Nat. Nanotechnol.* **12**, 430 (2017).
- L. Cui, S. Hur, Z. A. Akbar, J. C. Klöckner, W. Jeong, F. Pauly, S.-Y. Jang, P. Reddy, and E. Meyhofer, “Thermal conductance of single-molecule junctions,” *Nature* **572**, 628 (2019).
- N. Mosso, H. Sadeghi, A. Gemma, S. Sangtarash, U. Drechsler, C. Lambert, and B. Gotsmann, “Thermal transport through single-molecule junctions,” *Nano Lett.* **19**, 7614 (2019).
- N. Mosso, A. Prasmusinto, A. Gemma, U. Drechsler, L. Novotny, and B. Gotsmann, “Quantized thermal conductance in metallic heterojunctions,” *Appl. Phys. Lett.* **114**, 123102 (2019).
- M. A. Reed, C. Zhou, C. J. Muller, T. P. Burgin, and J. M. Tour, “Conductance of a molecular junction,” *Science* **278**, 252 (1997).
- P. Reddy, S.-Y. Jang, R. A. Segalman, and A. Majumdar, “Thermoelectricity in molecular junctions,” *Science* **315**, 1568 (2007).
- D. Xiang, X. Wang, C. Jia, T. Lee, and X. Guo, “Molecular-scale electronics: From concept to function,” *Chem. Rev.* **116**, 4318 (2016).
- L. Cui, R. Miao, C. Jiang, E. Meyhofer, and P. Reddy, “Perspective: Thermal and thermoelectric transport in molecular junctions,” *J. Chem. Phys.* **146**, 092201 (2017).
- N. Xin, J. Guan, C. Zhou, X. Chen, C. Gu, Y. Li, M. A. Ratner, A. Nitzan, J. F. Stoddart, and X. Guo, “Concepts in the design and engineering of single-molecule electronic devices,” *Nat. Rev. Phys.* **1**, 211 (2019).
- F. Evers, R. Korytár, S. Tewari, and J. M. Van Ruitenbeek, “Advances and challenges in single-molecule electron transport,” *Rev. Mod. Phys.* **92**, 035001 (2020).
- D. Segal and B. K. Agarwalla, “Vibrational heat transport in molecular junctions,” *Annu. Rev. Phys. Chem.* **67**, 185 (2016).
- B. Gotsmann, A. Gemma, and D. Segal, “Quantum phonon transport through channels and molecules—A perspective,” *Appl. Phys. Lett.* **120**, 160503 (2022).
- D. Segal, A. Nitzan, and P. Hänggi, “Thermal conductance through molecular wires,” *J. Chem. Phys.* **119**, 6840 (2003).
- R. Moghaddasi Fereidani and D. Segal, “Phononic heat transport in molecular junctions: Quantum effects and vibrational mismatch,” *J. Chem. Phys.* **150**, 024105 (2019).
- J. C. Klöckner, J. C. Cuevas, and F. Pauly, “Tuning the thermal conductance of molecular junctions with interference effects,” *Phys. Rev. B* **96**, 245419 (2017).
- J. C. Klöckner, M. Bürkle, J. C. Cuevas, and F. Pauly, “Length dependence of the thermal conductance of alkane-based single-molecule junctions: An *ab initio* study,” *Phys. Rev. B* **94**, 205425 (2016).
- Q. Li, I. Duchemin, S. Xiong, G. C. Solomon, and D. Donadio, “Mechanical tuning of thermal transport in a molecular junction,” *J. Phys. Chem. C* **119**, 24636 (2015).
- Q. Li, M. Strange, I. Duchemin, D. Donadio, and G. C. Solomon, “A strategy to suppress phonon transport in molecular junctions using π -stacked systems,” *J. Phys. Chem. C* **121**, 7175 (2017).
- M. Galperin, M. A. Ratner, and A. Nitzan, “Molecular transport junctions: Vibrational effects,” *J. Phys.: Condens. Matter* **19**, 103201 (2007).
- D. Dundas, E. J. McEniry, and T. N. Todorov, “Current-driven atomic waterwheels,” *Nat. Nanotechnol.* **4**, 99 (2009).
- J.-T. Lü, M. Brandbyge, and P. Hedegård, “Blowing the fuse: Berry’s phase and runaway vibrations in molecular conductors,” *Nano Lett.* **10**, 1657 (2010).
- Z. Huang, B. Xu, Y. Chen, M. D. Ventra, and N. Tao, “Measurement of current-induced local heating in a single molecule junction,” *Nano Lett.* **6**, 1240 (2006).
- D. R. Ward, D. A. Corley, J. M. Tour, and D. Natelson, “Vibrational and electronic heating in nanoscale junctions,” *Nat. Nanotechnol.* **6**, 33 (2011).
- Z. Ioffe, T. Shamai, A. Ophir, G. Noy, I. Yutsis, K. Kfir, O. Cheshnovsky, and Y. Selzer, “Detection of heating in current-carrying molecular junctions by Raman scattering,” *Nat. Nanotechnol.* **3**, 727 (2008).
- M. Tsutsui, M. Taniguchi, and T. Kawai, “Local heating in metal-molecule-metal junctions,” *Nano Lett.* **8**, 3293 (2008).
- C. Sabater, C. Untiedt, and J. M. van Ruitenbeek, “Evidence for non-conservative current-induced forces in the breaking of Au and Pt atomic chains,” *Beilstein J. Nanotechnol.* **6**, 2338 (2015).
- J.-T. Lü, S. Leatherer, N. R. Papior, and M. Brandbyge, “*Ab initio* current-induced molecular dynamics,” *Phys. Rev. B* **101**, 201406 (2020).
- C. Jia, A. Migliore, N. Xin, S. Huang, J. Wang, Q. Yang, S. Wang, H. Chen, D. Wang, B. Feng, Z. Liu, G. Zhang, D.-H. Qu, H. Tian, M. A. Ratner, H. Q. Xu, A. Nitzan, and X. Guo, “Covalently bonded single-molecule junctions with stable and reversible photoswitched conductivity,” *Science* **352**, 1443 (2016).
- D. Martínez Gutierrez, A. Di Pierro, A. Pecchia, L. M. Sandonas, R. Gutierrez, M. Bernal, B. Mortazavi, G. Cuniberti, G. Saracco, and A. Fina, “Thermal bridging of graphene nanosheets via covalent molecular junctions: A non-equilibrium Green’s functions–density functional tight-binding study,” *Nano Res.* **12**, 791 (2019).
- G. Li, B.-Z. Hu, N. Yang, and J.-T. Lü, “Temperature-dependent thermal transport of single molecular junctions from semiclassical Langevin molecular dynamics,” *Phys. Rev. B* **104**, 245413 (2021).
- J.-T. Lü, B.-Z. Hu, P. Hedegård, and M. Brandbyge, “Semi-classical generalized Langevin equation for equilibrium and nonequilibrium molecular dynamics simulation,” *Prog. Surf. Sci.* **94**, 21 (2019).
- L. Kantorovich, “Generalized Langevin equation for solids. I. Rigorous derivation and main properties,” *Phys. Rev. B* **78**, 094304 (2008).
- L. Kantorovich and N. Rompotis, “Generalized Langevin equation for solids. II. Stochastic boundary conditions for nonequilibrium molecular dynamics simulations,” *Phys. Rev. B* **78**, 094305 (2008).
- J.-S. Wang, “Quantum thermal transport from classical molecular dynamics,” *Phys. Rev. Lett.* **99**, 160601 (2007).
- W. Dou, G. Miao, and J. E. Subotnik, “Born-Oppenheimer dynamics, electronic friction, and the inclusion of electron-electron interactions,” *Phys. Rev. Lett.* **119**, 046001 (2017).
- J.-T. Lü, M. Brandbyge, P. Hedegård, T. N. Todorov, and D. Dundas, “Current-induced atomic dynamics, instabilities, and Raman signals: Quasiclassical Langevin equation approach,” *Phys. Rev. B* **85**, 245444 (2012).
- A. Stukowski, “Visualization and analysis of atomistic simulation data with OVITO—the open visualization tool,” *Modell. Simul. Mater. Sci. Eng.* **18**, 015012 (2010).
- L. Stella, C. D. Lorenz, and L. Kantorovich, “Generalized Langevin equation: An efficient approach to nonequilibrium molecular dynamics of open systems,” *Phys. Rev. B* **89**, 134303 (2014).
- H. Ness, L. Stella, C. D. Lorenz, and L. Kantorovich, “Applications of the generalized Langevin equation: Towards a realistic description of the baths,” *Phys. Rev. B* **91**, 014301 (2015).
- J. M. Soler, E. Artacho, J. D. Gale, A. Garcia, J. Junquera, P. Ordejón, and D. Sánchez-Portal, “The SIESTA method for *ab initio* order-N materials simulation,” *J. Phys.: Condens. Matter* **14**, 2745 (2002).
- M. Brandbyge, J. L. Mozos, P. Ordejón, J. Taylor, and K. Stokbro, “Density-functional method for nonequilibrium electron transport,” *Phys. Rev. B* **65**, 165401 (2002).

⁴³T. Frederiksen, M. Paulsson, M. Brandbyge, and A.-P. Jauho, “Inelastic transport theory from first principles: Methodology and application to nanoscale devices,” *Phys. Rev. B* **75**, 205413 (2007).

⁴⁴H. Wang, L. Zhang, J. Han, and W. E, “DeePMD-kit: A deep learning package for many-body potential energy representation and molecular dynamics,” *Comput. Phys. Commun.* **228**, 178 (2018).

⁴⁵D. Zhang, X. Zheng, and M. Di Ventra, “Local temperatures out of equilibrium,” *Phys. Rep.* **830**, 1 (2019).

⁴⁶J.-T. Lü, R. B. Christensen, J.-S. Wang, P. Hedegård, and M. Brandbyge, “Current-induced forces and hot spots in biased nanojunctions,” *Phys. Rev. Lett.* **114**, 096801 (2015).

⁴⁷C. Schirm, M. Matt, F. Pauly, J. C. Cuevas, P. Nielaba, and E. Scheer, “A current-driven single-atom memory,” *Nat. Nanotechnol.* **8**, 645 (2013).

⁴⁸T. Preis, S. Vrbica, J. Eroms, J. Repp, and J. M. van Ruitenbeek, “Current-induced one-dimensional diffusion of co adatoms on graphene nanoribbons,” *Nano Lett.* **21**, 8794 (2021).